sNucDrop-Seq: Dissecting cell-type composition and neuronal activity state in mammalian brains by massively parallel single-nucleus RNA-Seq

Peng Hu[1,2,*], Emily Fabyanic[1,2,*], Zhaolan Zhou[1,2], and Hao Wu[1,2,#]

[1]Department of Genetics, [2]Epigenetics Institute, Perelman School of Medicine, Philadelphia PA 19104, USA

*These authors contributed equally to this work

[#]To whom correspondence should be addressed

E-mail: haowu2@upenn.edu

Running Title: Massively parallel single-nucleus RNA-Seq analysis of mammalian brains

Massively parallel single-cell RNA sequencing can precisely resolve cellular diversity in a high-throughput manner at low cost, but unbiased isolation of intact single cells from complex tissues, such as adult mammalian brains, is challenging. Here, we integrate sucrose-gradient assisted nuclear purification with droplet microfluidics to develop a highly scalable single-nucleus RNA-Seq approach (sNucDrop-Seq), which is free of enzymatic dissociation and nucleus sorting. By profiling ~11,000 nuclei isolated from adult mouse cerebral cortex, we demonstrate that sNucDrop-Seq not only accurately reveals neuronal and non-neuronal subtype composition with high sensitivity, but also enables analysis of long non-coding RNAs and transient states such as neuronal activity-dependent transcription at single-cell resolution *in vivo*.

A fundamental challenge in deciphering cellular composition and cells' functional states in complex mammalian tissues manifests in the extraordinary diversity of cell morphology, size and local microenvironment. While current high-throughput single-cell RNA-Seq approaches have proved to be powerful tools for interrogating cell types, dynamic states and functional processes *in vivo* [1], these methods require the preparation of intact, single-cell suspensions from freshly isolated tissues, which is only practical for easily-dissociated embryonic and young postnatal tissues. This requirement poses an even greater challenge for cells with complex morphology such as mature neurons. Harsh enzymatic treatment not only favors recovery of easily dissociated cell types, but also introduces aberrant transcriptional changes during the dissociation process [2]. In addition, skeletal and cardiac muscle cells are frequently multinucleated and are large in size. For instance, each adult mouse skeletal muscle cell contains hundreds of nuclei and is ~5,000 μm in length and 10-50 μm in width [3]. Thus, existing high-throughput single-cell capture and library preparation methods, including isolation of cells by fluorescence activated cell sorting (FACS) into multi-well plates, sub-nanoliter wells, or droplet microfluidic encapsulation, are not optimized to accommodate these unusually large cells. Isolating individual nuclei for transcriptome analysis is a promising strategy, as single-nucleus RNA-Seq methods avoid strong biases against cells of complex morphology and large size [2,4-6], and can be potentially standardized to accommodate the study of various tissues. However, current single-nucleus RNA-Seq methods rely on fluorescence-activated nuclei sorting (FANS) [4,5] or Fluidigm

C1 [6] to capture nuclei, and thus cannot easily be scaled up to generate a comprehensive atlas of cell types in a given tissue, much less a whole organism.

An ideal solution to increase the throughput of single-nucleus RNA-Seq is to integrate nucleus purification with massively parallel single-cell RNA-Seq methods such as Drop-Seq [7], InDrop [8], or equivalent commercial platforms (e.g. 10x Genomics [9]). However, single-nucleus RNA-Seq is currently not supported on these droplet microfluidics platforms. Inhibitory effects due to cellular debris contamination and/or inefficient lysis of nuclear membranes might contribute to this failure. Historically, nuclei of high purity can be isolated from solid tissues or from cell lines with fragile nuclei by centrifugation through a dense sucrose cushion to protect nucleus integrity and strip away cytoplasmic contaminants. The sucrose gradient ultracentrifugation approach has been adapted to isolate neuronal nuclei for profiling histone modifications [10], nuclear RNA [11], and DNA methylation [11, 12] at genome-scale. To test whether this nuclei purification method supports single-nucleus RNA-Seq analysis, we isolated nuclei from cultured cells, as well as freshly isolated or frozen adult mouse brain tissues through douncing homogenization followed by sucrose gradient ultracentrifugation (**Fig. 1a and Supplementary Fig. 1**). After quality assessment and nuclei counting, we performed emulsion droplet barcoding of the nuclei and library preparation with both Drop-Seq and 10x Genomics platforms. While the10x Genomics single-cell 3' solution workflow supports cDNA amplification only from whole cells (possibly due to inefficient lysis of nuclear membrane), the Drop-Seq platform yielded high quality cDNA and sequencing libraries from both whole cells and nuclei (freshly isolated or frozen samples) (**Supplementary Fig. 2**). These results suggest that nucleus purification and nuclear membrane lysis are critical factors for efficient library preparation in single-nucleus RNA-Seq.

We next validated the specificity of sucrose gradient-assisted single-nucleus Drop-Seq (sNucDrop-Seq) with species-mixing experiments, using nuclei isolated from *in vitro* cultured mouse and human cells. This analysis indicates that the rate of co-encapsulation of multiple nuclei per droplet (~2.6%) is comparable to standard Drop-Seq (**Supplementary Fig. 3a**). To assess the sensitivity of sNucDrop-Seq, we performed shallow sequencing of cultured mouse 3T3 cells at either single-cell (with Drop-Seq: detecting on average 3,325 genes with ~25,000 reads per cell for 1,160 cells with >800 genes detected) or single-nucleus (with sNucDrop-Seq:

detecting on average 2,665 genes with ~23,000 reads per nucleus for 1,984 nuclei with >800 genes detected) resolution (**Fig. 1b**). With standard Drop-Seq microfluidics devices and flow parameters, the throughput of sNucDrop-Seq (1.9%, 1,829 / 95,000 barcoded beads) is comparable to that of Drop-Seq (1.5%, 1,160 / 77,000 barcoded beads). Comparative analysis of Drop-Seq and sNucDrop-Seq reveals that mitochondria-derived RNAs (e.g. *mt-Nd1*, *mt-Nd2*) and nucleus-enriched long-noncoding RNAs (e.g. *Malat1*) were enriched in cytoplasmic and nuclear compartments, respectively (**Supplementary Fig. 3b**). Thus, integrating sucrose gradient centrifugation-based nuclei purification with the current Drop-Seq microfluidics device and workflow may support massively parallel single-nucleus RNA-Seq.

To demonstrate the utility of sNucDrop-Seq in studying complex adult tissues, we analyzed nuclei isolated from adult mouse cerebral cortex. The average expression profiles of single nuclei from two biologically independent replicates were well correlated (r=0.993; **Supplementary Fig. 3c**). Out of reads uniquely mapped to the genome (78.0% of all reads), 76.3% of reads were aligned to the expected strand of genic regions (25.3% exonic and 51.0% intronic), and the remaining 23.7% to intergenic regions or to the opposite strand of annotated genic regions. The relatively high proportion of intronic reads is similar to previous single-nucleus RNA-Seq study of human cortex (~48.7%) [5], reflecting the enrichment of nascent, pre-processed transcripts in the nucleus. Because most exonic (91.4%) and intronic (86.0%) reads were mapped to the expected strand of annotated transcripts, we retained both exonic and intronic reads for downstream analyses. After quality filtering, we retained 10,996 nuclei (~20,000 uniquely mapped reads per nucleus) from 13 animals, detecting, on average, 4,273 transcripts (unique molecular identifiers [UMIs]), and 1,831 genes per nucleus (**Fig. 1b**). After correcting for batch effects, we identified highly variable genes, and determined significant principal components (PC) with these variable genes. We then performed graph-based clustering and visualized distinct groups of cells using non-linear dimensionality reduction with spectral *t*-distributed stochastic neighbor embedding (tSNE) (**Methods**). This initial analysis segregated nuclei into 19 distinct clusters (**Fig. 1c**). Each cluster contains nuclei from multiple animals, indicating the transcriptional identities of these cell-type-specific clusters are reproducible across biological replicates (**Supplementary Fig. S4a**).

On the basis of known markers for major cell types, we identified 10 excitatory neuronal clusters (Ex 1-10; *Slc17a7*$^{+}$), four inhibitory neuronal clusters (Inh 1-4; *Gad1*$^{+}$), and five non-neuronal clusters (astrocytes [Astro; *Gja1*$^{+}$], oligodendrocyte precursor cells [OPC; *Pdgfra*$^{+}$], oligodendrocytes [oligo; *Mog*$^{+}$], microglia [MG; *Ctss*$^{+}$], and endothelial cells [EC; *Flt1*$^{+}$]) (**Fig. 1c-d** and **Supplementary Fig. 4b**). We readily uncovered all major subtypes of GABAergic inhibitory neurons expressing known canonical markers: *Sst* (somatostatin; cluster Inh1), *Pvalb* (parvalbumin; cluster Inh2), *Vip* (vasoactive intestinal peptide; cluster Inh3) and *Ndnf* (neuron-derived neurotrophic factor; cluster Inh4) (**Supplementary Fig. 5a**). For glutamatergic excitatory neurons, hierarchical clustering grouped the ten clusters into two major groups (**Fig. 1e**), largely corresponding to their cortical layer positions, from superficial (cluster Ex1-5: L2/3 and L4) to deep (cluster Ex6-10: L5a/b and L6a/b) layers (**Fig. 1d** and **Supplementary Fig. 5**). Consistent with previous studies [5, 13, 14], we readily annotated anatomical location of each excitatory neuronal cluster *post-hoc* by its expression of known layer-specific marker genes (**Supplementary Fig. 6a-b**). In addition to protein-coding marker genes, we have also identified a list of long non-coding RNAs that are specifically expressed in distinct cell clusters (**Fig. 1e** and **Supplementary Fig. 5b**). For instance, *1700016P03Rik* is specifically detected in cluster Ex5, and this non-coding transcript acts mainly as a primary transcript encoding two neuronal activity-regulated microRNAs (*Mir212* and *Mir132*) [15, 16] (**Supplementary Fig. 7**), which is consistent with the enrichment of other activity-dependent genes (*Fos, Arc, Npas4*) in this excitatory neuronal cluster (**Supplementary Fig. 6a**), and raises the possibility that Ex5 is enriched of activated neurons (see below). The identification of both protein-coding and non-coding transcripts as cell-type-specific markers highlights the potential of sNucDrop-Seq in exploring the emerging role of non-coding RNAs at single-cell resolution *in vivo*.

Cortical interneurons are highly diverse in terms of morphology, connectivity and physiological properties [17]. To further annotate these inhibitory neuronal subtypes, we performed sub-clustering on the 876 inhibitory neuronal nuclei in our dataset, identifying eight sub-clusters (cluster A-H in **Fig. 2a**). Unlike previous single-cell RNA-Seq analysis that employed pre-enrichment of cortical inhibitory neurons from transgenic mouse lines [18], sNucDrop-Seq samples the nuclei in proportion to cells' abundance in their native environment, which provides a more accurate description of the cellular composition at the transcriptomic level. This analysis

identified *Pvalb*-expressing subtypes (cluster D and E; *n*=359/876 nuclei, 41.0%) and *Sst*-expressing subtypes (cluster F, G, H; *n*=304/876 nuclei, 34.7%) as two major groups of cortical interneurons (**Fig. 2b-d**), in accordance with previous observations derived from *in situ* hybridization (ISH)- or immunostaining-based methods that *Pvalb*- and *Sst*-positive groups account for ~40% and ~30% of interneurons, respectively, in the neocortex [19]. Beyond the major interneuron subtypes, we identified one *Ndnf*-expressing subtype (cluster A; *n*=84/876 nuclei), one *Vip*-expressing subtype (cluster B; *n*=74/876 nuclei), and one synuclein gamma (*Sncg*)-expressing subtype (cluster C; *n*=55/876 nuclei) (**Fig. 2b-d** and **Supplementary Fig. 8a**). On the basis of combinatorial expression of known marker genes associated with specific cortical layer and developmental origin, interneuron subtypes identified by sNucDrop-Seq parallel those identified from previous studies of mouse or human cortex [5, 18], revealing inhibitory neuronal heterogeneity in both cortical layer distribution (**Supplementary Fig. 8a-b**) and the developmental origin from subcortical regions of the medial or caudal ganglionic eminences (MGE or CGE) (**Fig. 2e**). Therefore, sNucDrop-Seq is able to resolve cellular heterogeneity and quantify cell-type composition at transcriptomic level with high sensitivity, including rare interneuron subtypes.

For glutamatergic neurons, unsupervised graph-based sub-clustering of two groups of excitatory neurons (upper layers versus lower layers) identified a total of 18 subtypes (Upper Ex 1-11 and Lower Ex 1-7; **Fig. 3a**). We associated each excitatory neuronal sub-cluster with a distinct combination of known markers indicative of their superficial-to-deep layer distribution (**Supplementary Fig. 9a**), capturing finer distinctions between closely related subtypes in each cortical layer, which is in high concordance with subtypes previously identified in human [5] and mouse [14, 18] cortices (**Fig. 3b** and **Supplementary Fig. 9b**). Beyond excitatory neuronal subtypes defined by cortical layer-specific markers, our analysis also resolved heterogeneity in neuronal activation states. In response to an activity-inducing experience, cortical excitatory neurons express a complex program of activity-dependent genes [20]. Both upper-Ex3 (n=209; 3.1% of 6,770 nuclei in upper layer sub-clusters) and lower-Ex5 (n=213; 8.1% of 2,642 nuclei in lower layer sub-clusters) neurons are specifically associated with high-level expression of activity-dependent genes (**Fig. 3b** and **Supplementary Fig. 9c**), including immediately early genes (IEGs) such as *Fos*, *Arc*, and *Egr1* as well as other activity-regulated transcription factors (e.g.

Npas4), genes encoding proteins that function at synapses (e.g. *Homer1*), and non-coding RNAs (e.g. *1700016P03Rik* that encodes Mir132). We determined the genes specifically enriched in upper-Ex3 (*n*=160 genes, as compared to other upper-Ex sub-clusters) or lower-Ex5 (*n*=134 genes, as compared to other lower-Ex sub-clusters) neurons (**Fig. 3c**). Transcriptional signatures identified in these two sub-populations are enriched for genes involved in the MAPK signaling pathway (e.g. *Dusp1*; adjusted $P=2.67\text{x}10^{-2}$ for upper-Ex3 sub-cluster), as previously reported in low-throughput single-nucleus RNA-Seq analysis of *Fos*-positive nuclei isolated from the hippocampus of adult mice exposed to a novel environment [2]. Together, these results demonstrate the utility of sNucDrop-Seq in the identification of transient transcriptional states, such as neuronal activation.

In conclusion, sNucDrop-Seq is a robust approach for massively parallel analysis of nuclear RNAs at single-cell resolution. Because intact nuclei isolation can potentially be accomplished by mechanical douncing and sucrose gradient ultracentrifugation in almost any primary tissue, including frozen archived human tissues, sNucDrop-Seq and similar approaches pave the way to systematically identify cell-types, reveal subtype composition, and dissect transient functional states such as activity-dependent transcription in complex mammalian tissues.

ACKNOWLEDGEMENTS

Z.Z is supported by NIH grant R56MH111719. H.W. is supported by the National Human Genome Research Institute (R00HG007982).

AUTHOR CONTRIBUTIONS

H.W. and Z.Z. conceived the project. H.W., P.H. and E.F. performed experiments and carried out data analysis. H.W. wrote the manuscript.

References

1. Tanay, A. & Regev, A. Scaling single-cell genomics from phenomenology to mechanism. *Nature* **541**, 331-338 (2017).
2. Lacar, B. et al. Nuclear RNA-seq of single neurons reveals molecular signatures of activation. *Nat Commun* **7**, 11022 (2016).
3. White, R.B., Bierinx, A.S., Gnocchi, V.F. & Zammit, P.S. Dynamics of muscle fibre growth during postnatal mouse development. *BMC Dev Biol* **10**, 21 (2010).
4. Habib, N. et al. Div-Seq: Single-nucleus RNA-Seq reveals dynamics of rare adult newborn neurons. *Science* **353**, 925-928 (2016).
5. Lake, B.B. et al. Neuronal subtypes and diversity revealed by single-nucleus RNA sequencing of the human brain. *Science* **352**, 1586-1590 (2016).
6. Zeng, W. et al. Single-nucleus RNA-seq of differentiating human myoblasts reveals the extent of fate heterogeneity. *Nucleic Acids Res* **44**, e158 (2016).
7. Macosko, E.Z. et al. Highly Parallel Genome-wide Expression Profiling of Individual Cells Using Nanoliter Droplets. *Cell* **161**, 1202-1214 (2015).
8. Klein, A.M. et al. Droplet barcoding for single-cell transcriptomics applied to embryonic stem cells. *Cell* **161**, 1187-1201 (2015).
9. Zheng, G.X. et al. Massively parallel digital transcriptional profiling of single cells. *Nat Commun* **8**, 14049 (2017).
10. Jiang, Y., Matevossian, A., Huang, H.S., Straubhaar, J. & Akbarian, S. Isolation of neuronal chromatin from brain tissue. *BMC Neurosci* **9**, 42 (2008).
11. Mo, A. et al. Epigenomic Signatures of Neuronal Diversity in the Mammalian Brain. *Neuron* **86**, 1369-1384 (2015).
12. Lister, R. et al. Global epigenomic reconfiguration during Mammalian brain development. *Science* **341**, 1237905 (2013).
13. Madisen, L. et al. Transgenic mice for intersectional targeting of neural sensors and effectors with high specificity and performance. *Neuron* **85**, 942-958 (2015).
14. Zeisel, A. et al. Brain structure. Cell types in the mouse cortex and hippocampus revealed by single-cell RNA-seq. *Science* **347**, 1138-1142 (2015).
15. Nudelman, A.S. et al. Neuronal activity rapidly induces transcription of the CREB-regulated microRNA-132, in vivo. *Hippocampus* **20**, 492-498 (2010).
16. Aten, S., Hansen, K.F., Hoyt, K.R. & Obrietan, K. The miR-132/212 locus: a complex regulator of neuronal plasticity, gene expression and cognition. *RNA Dis* **3** (2016).
17. Kepecs, A. & Fishell, G. Interneuron cell types are fit to function. *Nature* **505**, 318-326 (2014).
18. Tasic, B. et al. Adult mouse cortical cell taxonomy revealed by single cell transcriptomics. *Nat Neurosci* **19**, 335-346 (2016).
19. Rudy, B., Fishell, G., Lee, S. & Hjerling-Leffler, J. Three groups of interneurons account for nearly 100% of neocortical GABAergic neurons. *Dev Neurobiol* **71**, 45-61 (2011).
20. Ebert, D.H. & Greenberg, M.E. Activity-dependent neuronal signalling and autism spectrum disorder. *Nature* **493**, 327-337 (2013).

Figure Legends

Figure 1. sNucDrop-Seq: a massively parallel single-nucleus RNA-Seq method.

(**a**) Overview of sNucDrop-Seq. Step 1, dounce homogenization in lysis buffer is used to disrupt cellular membranes; Step2, nuclei are purified from cellular debris through sucrose gradient ultracentrifugation; Step3, quality and yield of nuclei is determined by hemocytometer count; Step4, nuclei and barcoded beads are co-encapsulated by an emulsion-droplet microfluidic device. Red arrows indicate representative nuclei before or after sucrose gradient centrifugation.

(**b**) Violin plots illustrating number of transcripts (UMIs) detected by sNucDrop-Seq of nuclei isolated from mouse 3T3 cells (~23,000 reads per nucleus) and adult mouse cortex (~20,000 reads per nucleus) or by Drop-Seq of whole cells from 3T3 cells (~25,000 reads per cell). Center line: median; circle: mean; limits: first and third quartile; whiskers, ±1.5 IQR. Indicated on top are the number of cells or nuclei (>= 800 genes detected), mean number of UMIs per cells/nuclei, and mean number of genes per cells/nuclei.

(**c**) Two-dimensional spectral t-stochastic neighborhood embedding (tSNE) plot of 11,283 nuclei isolated from adult mouse cortex, colored per density clustering and annotated according to known cell types. Ex, excitatory neurons; Inh, inhibitory neurons; Astro, astrocytes; OPC, oligodendrocyte precursor cells; Oligo, oligodendrocytes; MG, microglia; EC, endothelial cells.

(**d**) Marker gene expression shown by re-coloring the tSNE plot. Shown is the same plot as Fig. 1c but with nuclei colored by the expression level of known cell type (e.g. Ex, Inh, Astro, Oligo, EC)- or cortical layer (L2/3/4/5/6)-specific marker genes.

(**e**) Dendrogram illustrating relatedness of cell clusters, followed by (from left to right) cluster identification (ID), cell number per major cell type, UMIs per cluster (mean ± s.e.m.), number of genes detected per cluster (mean ± s.e.m.), heatmap showing protein-coding marker genes, and heatmap showing long non-coding RNA markers.

Figure 2. sNucDrop-Seq reveals inhibitory neuronal subtypes and composition.

(**a**) Spectral tSNE plot of 876 inhibitory neurons, colored according to the results of sub-clustering (thumbnail: Fig. 1c).

(**b**) Marker gene expression shown by re-coloring tSNE plot. Shown is the same plot as Fig. 2a but with nuclei colored by the expression level of known inhibitory neuronal subtype-specific marker genes.

(**c**) Violin plots showing select marker gene expression for inhibitory neuronal subtypes. Five mutually exclusive subtype-specific marker genes are highlighted in red.

(**d**) Summary of inhibitory neuronal subtypes identified by sNucDrop-Seq. GABAergic subtypes are grouped according to five major classes. Also shown are number of nuclei per subtype and representative marker genes for each subtype.

(**e**) Heatmap showing select marker genes that distinguish inhibitory neurons originated from either CGE or MGE.

Figure 3. Excitatory neuronal subtypes resolve heterogeneity in cortical layer distribution and state of neuronal activity.

(**a**) Spectral tSNE plots of 6,770 upper and 2,642 lower layer excitatory neurons, colored according the results of sub-clustering (thumbnails: Fig. 1c).

(**b**) Heatmap for layer-specific markers and neuronal activity-regulated genes showing cortical layer identity (L2/3/, L4, L5a/b, L6a/b), excitatory subtypes, and activity-induced gene expression.

(**c**) Differential expression between activated and inactivated excitatory neurons within upper (left) or lower (right) layer sub-clusters. Significant genes (red or blue), genes with p-values less than 0.001 and absolute natural log fold changes greater than 0.25. Violin plots showing select marker gene expression. #, denotes that the expression of *Bdnf* is not significantly different between active and inactive lower layer excitatory neurons. *, denotes that *Epha6* and *Lingo2* were expressed at significantly higher level in inactive lower layer excitatory neurons compared to active counterparts.

Figure 1

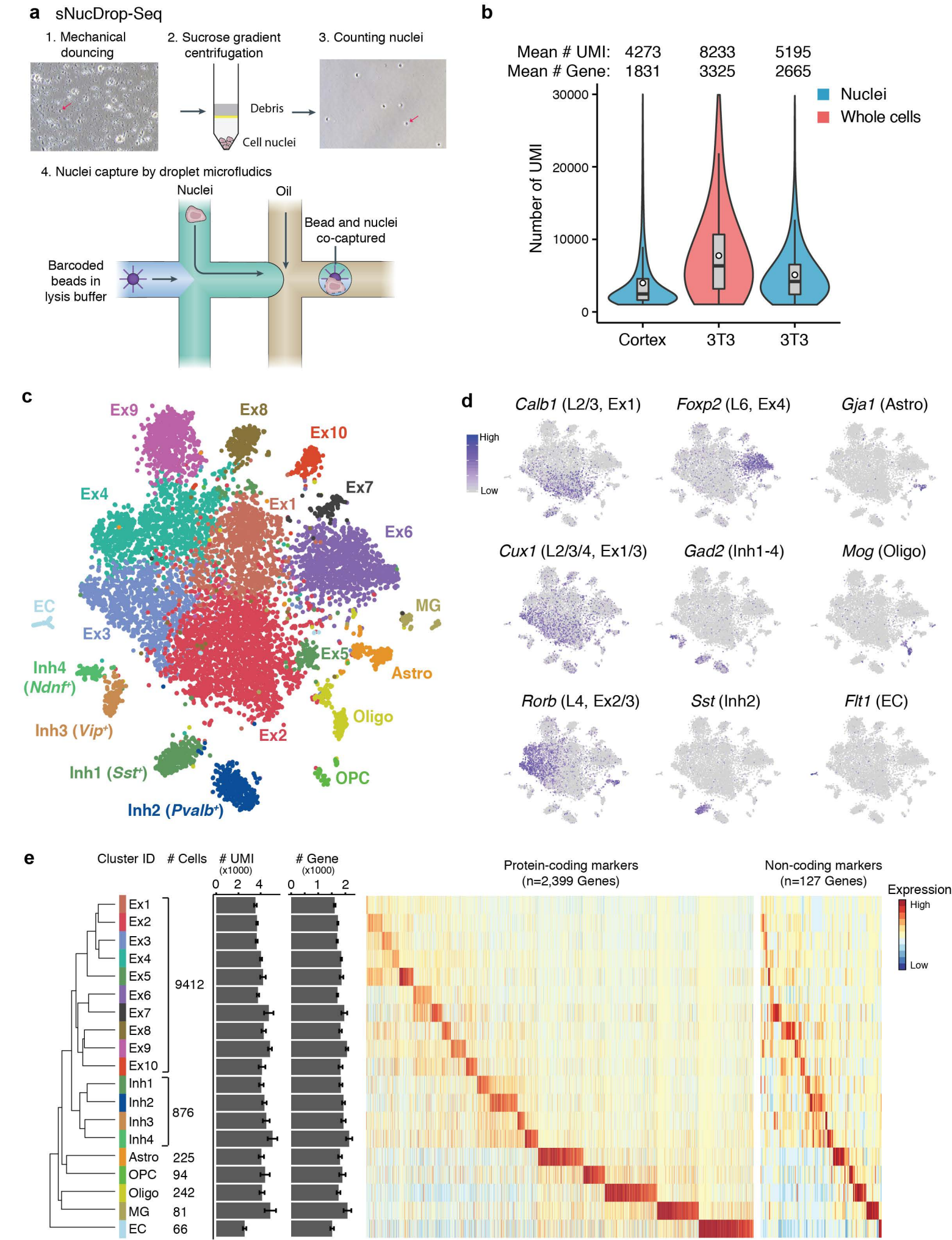

Figure 2

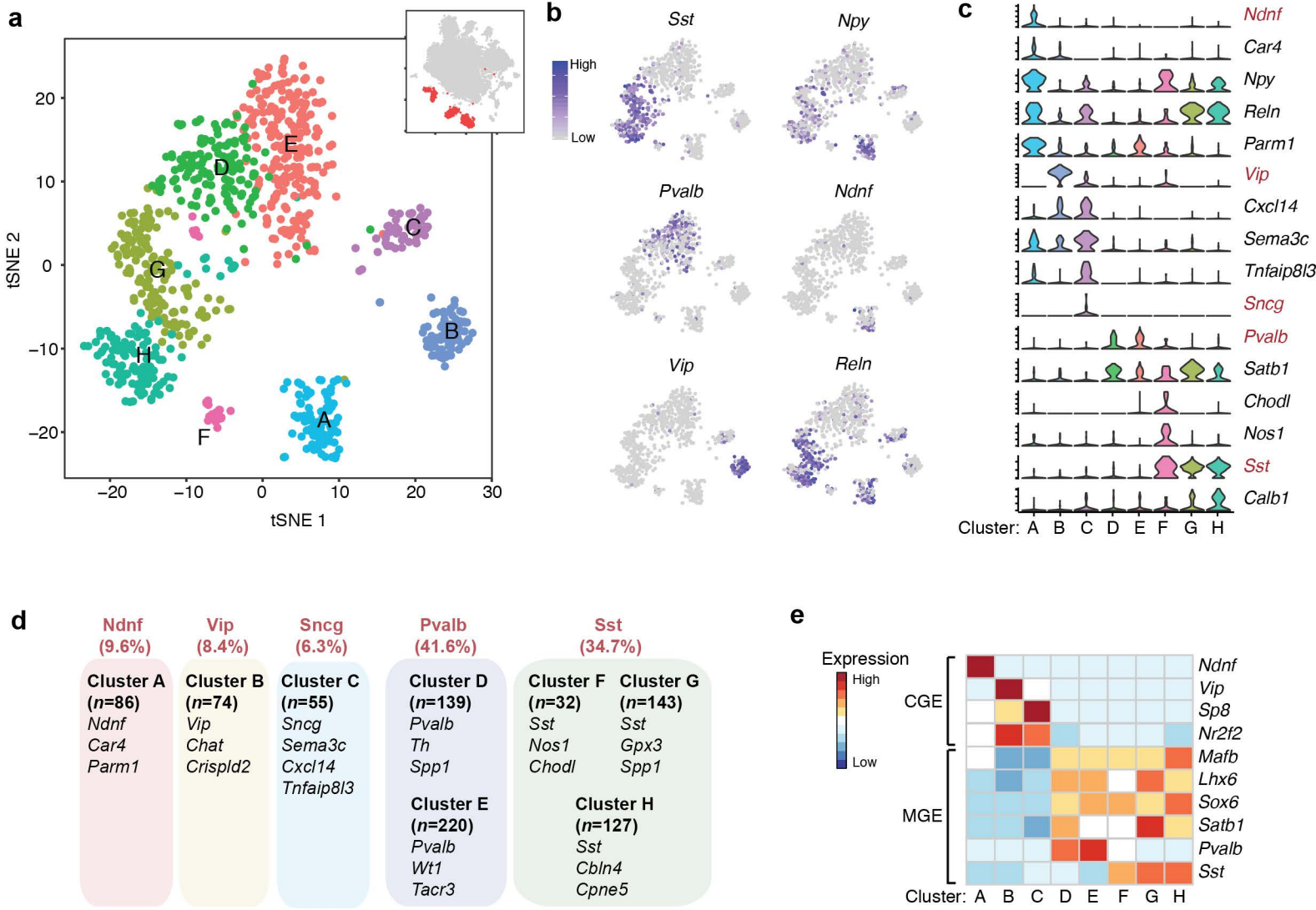
a
tSNE 1
tSNE 2
A
B
C
D
E
F
G
H
b
Sst
Npy
Pvalb
Ndnf
Vip
Reln
High
Low
c
Ndnf
Car4
Npy
Reln
Parm1
Vip
Cxcl14
Sema3c
Tnfaip8l3
Sncg
Pvalb
Satb1
Chodl
Nos1
Sst
Calb1
Cluster: A B C D E F G H
d
Ndnf (9.6%)
Cluster A (n=86)
Ndnf
Car4
Parm1
Vip (8.4%)
Cluster B (n=74)
Vip
Chat
Crispld2
Sncg (6.3%)
Cluster C (n=55)
Sncg
Sema3c
Cxcl14
Tnfaip8l3
Pvalb (41.6%)
Cluster D (n=139)
Pvalb
Th
Spp1
Cluster E (n=220)
Pvalb
Wt1
Tacr3
Sst (34.7%)
Cluster F (n=32)
Sst
Nos1
Chodl
Cluster G (n=143)
Sst
Gpx3
Spp1
Cluster H (n=127)
Sst
Cbln4
Cpne5
e
Expression
High
Low
CGE
MGE
Ndnf
Vip
Sp8
Nr2f2
Mafb
Lhx6
Sox6
Satb1
Pvalb
Sst
Cluster: A B C D E F G H

Figure 3

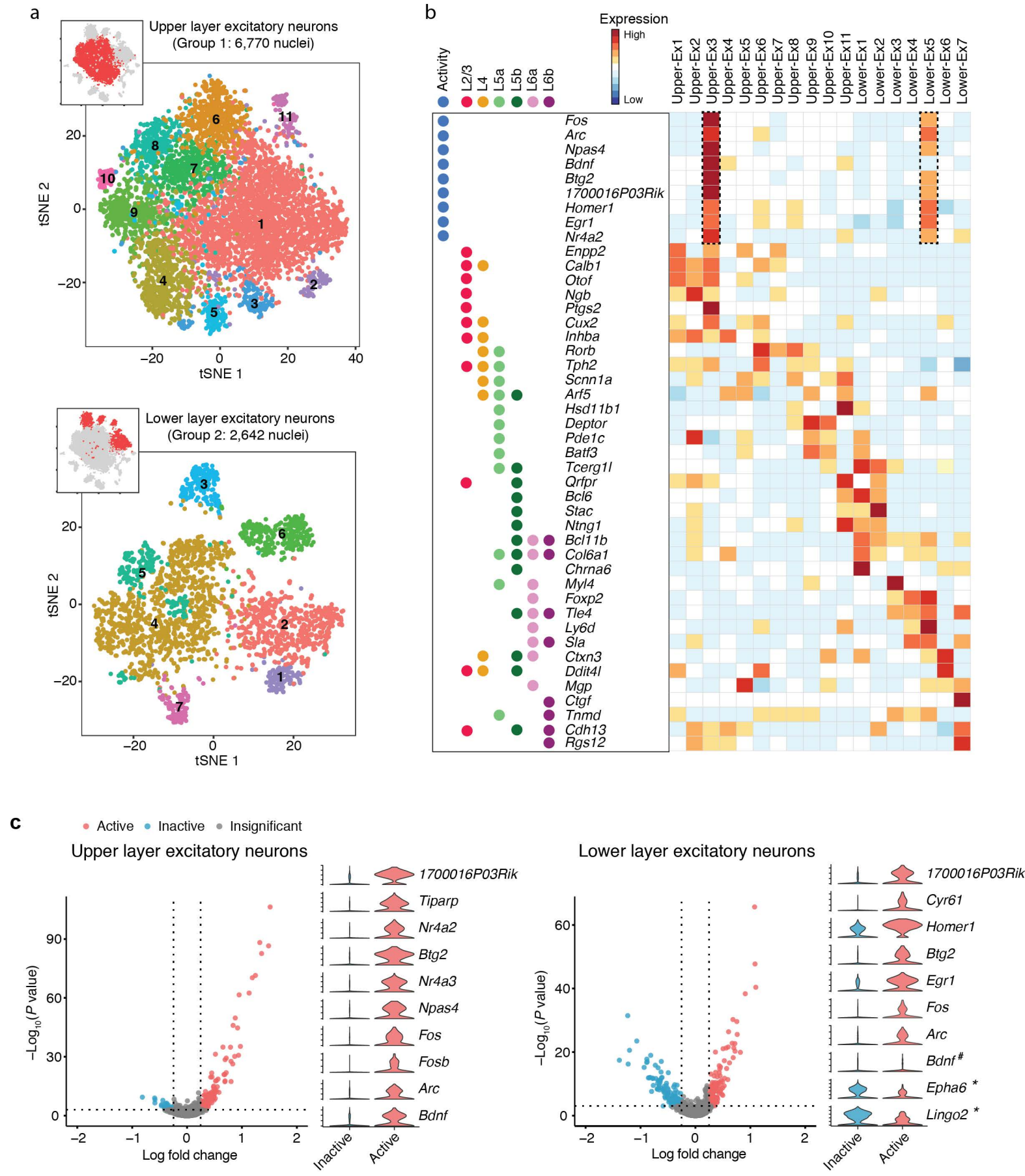
a
Upper layer excitatory neurons
(Group 1: 6,770 nuclei)
tSNE 2
tSNE 1
Lower layer excitatory neurons
(Group 2: 2,642 nuclei)
b
Expression
High
Low
Activity
L2/3
L4
L5a
L5b
L6a
L6b
Upper-Ex1
Upper-Ex2
Upper-Ex3
Upper-Ex4
Upper-Ex5
Upper-Ex6
Upper-Ex7
Upper-Ex8
Upper-Ex9
Upper-Ex10
Upper-Ex11
Lower-Ex1
Lower-Ex2
Lower-Ex3
Lower-Ex4
Lower-Ex5
Lower-Ex6
Lower-Ex7
Fos
Arc
Npas4
Bdnf
Btg2
1700016P03Rik
Homer1
Egr1
Nr4a2
Enpp2
Calb1
Otof
Ngb
Ptgs2
Cux2
Inhba
Rorb
Tph2
Scnn1a
Arf5
Hsd11b1
Deptor
Pde1c
Batf3
Tcerg1l
Qrfpr
Bcl6
Stac
Ntng1
Bcl11b
Col6a1
Chrna6
Myl4
Foxp2
Tle4
Ly6d
Sla
Ctxn3
Ddit4l
Mgp
Ctgf
Tnmd
Cdh13
Rgs12
c
Active
Inactive
Insignificant
Upper layer excitatory neurons
−Log10(P value)
Log fold change
1700016P03Rik
Tiparp
Nr4a2
Btg2
Nr4a3
Npas4
Fos
Fosb
Arc
Bdnf
Inactive
Active
Lower layer excitatory neurons
−Log10(P value)
Log fold change
1700016P03Rik
Cyr61
Homer1
Btg2
Egr1
Fos
Arc
Bdnf #
Epha6 *
Lingo2 *
Inactive
Active